Beamforming and Combining Strategies for MIMO-OFDM over Doubly Selective Channels

Sibasish Das and Philip Schniter
Dept. ECE, The Ohio State University
Columbus, OH 43210
{dass,schniter}@ece.osu.edu

***Abstract*— Beamforming and combining strategies are extensively used to harness spatial diversity gains in MIMO-OFDM systems. However, traditional approaches are ineffective when time-variations in the underlying wireless channel introduce inter-carrier interference (ICI). We propose novel beamforming and combining strategies for such time- and frequency-selective wireless channels. Results show that our schemes enjoy large gains over traditional approaches. Additionally, we find that our schemes are robust to the use of predicted (as opposed to perfect) channel state information at the transmitter.**[1]

I. Introduction

The last decade has seen the emergence of multiple-input multiple-output (MIMO) systems that provide large spatial diversity gains [1]–[3]. MIMO systems promise a diversity advantage proportional to the product of the number of transmit and receive antennas. Space-time codes [1], [2] and, more recently, lattice codes [4] have been shown to take advantage of spatial diversity. When channel state information (CSI) is available at the transmitter, one can also combine traditional coding techniques with beamforming and antenna combining to leverage spatial diversity (see [3], [5] and references therein).

Multi-carrier modulation (MCM) [6]–[9] has emerged as an attractive strategy for frequency-selective wireless channels. Orthogonal frequency-division multiplexing (OFDM) is arguably the most popular MCM scheme [6], [10], transforming the inter-symbol interference (ISI)-inducing frequency-selective channel into a set of independent parallel sub-channels. When multiple antennas are available at the transmitter and/or receiver in an OFDM system, spatial diversity can also be harnessed via beamforming and combining (see, e.g., [11]–[13]).

One of the central assumptions in traditional MIMO-OFDM beamforming and combining is that *sub-carriers do not interfere* and, hence, the signal to noise ratio (SNR) for each sub-carrier can be maximized independently. However, some of tomorrow's high-rate systems can be expected to function in a highly mobile environment, where the underlying wireless channel is time-selective in addition to frequency-selective, i.e., doubly selective (DS). In such channels, the time variations can cause substantial inter-carrier interference (ICI) [14]–[16], rendering traditional MIMO-OFDM beamforming and combining ineffective. Our goal here is to develop novel MIMO-OFDM beamforming and combining strategies that are effective even in the presence of significant ICI.

[1]This work was supported by Motorola, Inc.

In this paper, we design beamforming and combining strategies for MIMO-OFDM that boost the (ergodic) achievable rate for a MIMO-OFDM system employing low-complexity local frequency-domain processing. The paper is organized as follows: Sec. II describes the system model, Sec. III details the beamforming and combining strategies, Sec. IV presents and discusses numerical results, and Sec. V concludes.

Notation: In the paper, we use $(\cdot)^T$ to denote transpose and $(\cdot)^H$ conjugate transpose. $\mathcal{D}(\boldsymbol{A}_0,\cdots,\boldsymbol{A}_{N-1})$ denotes the matrix constructed by placing matrices $\{\boldsymbol{A}_k\}_{k=0}^{N-1}$ diagonally. $[\boldsymbol{B}]_{m,n}$ denotes the element in the m^{th} row and n^{th} column of $\boldsymbol{B}$, where row/column indices begin with zero. $\boldsymbol{I}_K$ denotes the $K\times K$ identity matrix and $\boldsymbol{J}_{K_1,K_2}(k_1,k_2)$ the $K_1\times K_2$ matrix with only one non-zero entry: $[\boldsymbol{J}_{K_1,K_2}(k_1,k_2)]_{k_1,k_2}=1$. The principal eigenvector of a positive definite matrix $\boldsymbol{A}$ is denoted by $\boldsymbol{\nu}_*(\boldsymbol{A})$ and the Kronecker product by $\otimes$. Also, $\langle\cdot\rangle_N$ denotes the modulo-N operation, and $\mathbb{C}$ the set of all complex numbers. Expectation is denoted by $\mathrm{E}(\cdot)$ and auto-covariance by $\boldsymbol{\Sigma}_{\boldsymbol{b}}:=E(\boldsymbol{b}\boldsymbol{b}^H)-E(\boldsymbol{b})E(\boldsymbol{b}^H)$.

II. System Model

In this paper, a beamforming MIMO-OFDM system with N_t transmit antennas, N_r receive antennas and N sub-carriers is referred to as an (N_t,N_r,N) MIMO-OFDM system. In the considered system, we assume that coding is done over large blocks of N_b OFDM symbols, that coding is done independently for each sub-carrier using i.i.d. (complex) Gaussian codebooks, and that an average power constraint is enforced. Thus, in the beamforming (N_t,N_r,N) MIMO-OFDM system, the i^{th} OFDM symbol is $\boldsymbol{s}(i)=[s_0(i),s_1(i),\cdots,s_{N-1}(i)]^T$, where $s_k(i)$ is the i^{th} symbol of the codeword on the k^{th} sub-carrier. The average power constraint and the use of i.i.d. Gaussian codebooks implies that each OFDM symbol is zero mean i.i.d. complex Gaussian distributed with $\boldsymbol{\Sigma}_{\boldsymbol{s}}=\boldsymbol{I}_N$. The i^{th} MIMO-OFDM symbol $\boldsymbol{t}(i)\in\mathbb{C}^{NN_t}$ is defined as $\boldsymbol{t}(i):=[\underline{\boldsymbol{t}}_0^T(i),\underline{\boldsymbol{t}}_1^T(i),\cdots,\underline{\boldsymbol{t}}_{N-1}^T(i)]^T$, where the entries of vector $\underline{\boldsymbol{t}}_k(i)\in\mathbb{C}^{N_t}$ are modulated onto the k^{th} sub-carrier at the N_t transmit antennas. For the considered system, the set of beamforming vectors (BVs), $\{\boldsymbol{x}_k(i)\in\mathbb{C}^{N_t}\}_{k=0}^{N-1}$, relate the i^{th} OFDM symbol to the i^{th} MIMO-OFDM symbol as

$$\boldsymbol{t}(i) \;=\; \mathcal{D}\big(\boldsymbol{x}_0(i),\boldsymbol{x}_1(i),\cdots,\boldsymbol{x}_{N-1}(i)\big)\boldsymbol{s}(i). \qquad (1)$$

Recall that we have enforced an average power constraint and that each codeword is spread over a large number of N_b OFDM symbols. As the channel experienced by each sub-carrier is statistically identical over this block of N_b symbols, it is assumed that $||\boldsymbol{x}_k(i)|| = 1$, for all k and i. Components of $\boldsymbol{t}(i)$ are collected along the respective transmit antenna, modulated using an IFFT and transmitted after the addition of a cyclic-prefix (CP).

The signal transmitted from the k_t^{th} transmit antenna encounters a wireless channel en route to the k_r^{th} receive antenna. Each such wireless channel is modeled as Rayleigh faded with a delay spread of N_h chips, a uniform power profile, and a (chip normalized) single-sided maximum Doppler spread of $f_{\mathsf{d}}T_c$. Moreover, all spatial paths are assumed to suffer independent fades and satisfy the wide sense stationary uncorrelated scattering (WSSUS) property. At each receive antenna, an FFT is taken on the observations after removal of the CP. The resulting frequency domain observation for the i^{th} OFDM symbol is $\boldsymbol{r}(i) := [\underline{\boldsymbol{r}}_0^T(i), \underline{\boldsymbol{r}}_1^T(i), \cdots, \underline{\boldsymbol{r}}_{N-1}^T(i)]^T$, where entries of $\underline{\boldsymbol{r}}_k(i) \in \mathbb{C}^{N_r}$ are the observations on the k^{th} sub-carrier at the N_r receive antennas. The observation $\boldsymbol{r}(i)$ can be expressed as

$$\boldsymbol{r}(i) = \boldsymbol{H}(i)\mathcal{D}\Big(\boldsymbol{x}_0(i), \boldsymbol{x}_1(i), \cdots, \boldsymbol{x}_{N-1}(i)\Big)\boldsymbol{s}(i) + \boldsymbol{w}(i), \quad (2)$$

where $\boldsymbol{w}(i)$ are samples of zero mean additive white complex Gaussian noise with covariance $\boldsymbol{\Sigma}_{\boldsymbol{w}} = \sigma^2 \boldsymbol{I}_{NN_r}$ and $\boldsymbol{H}(i) \in \mathbb{C}^{N_r N \times N_t N}$ is the MIMO frequency domain channel matrix (FDCM). This MIMO-FDCM can be obtained by

$$\boldsymbol{H} \;=\; \sum_{k_r, k_t} \boldsymbol{\mathcal{H}}_{k_r,k_t}(i) \otimes \boldsymbol{J}_{N_r,N_t}(k_r, k_t), \quad (3)$$

where $\boldsymbol{\mathcal{H}}_{k_r,k_t}(i) \in \mathbb{C}^{N \times N}$ is the sub-carrier coupling matrix (SCM) for transmission from the k_t^{th} transmit to the k_r^{th} receive antenna. That is, $[\boldsymbol{\mathcal{H}}_{k_r,k_t}(i)]_{m_1,m_2}$ represents the influence of the component of $\underline{\boldsymbol{t}}_{m_2}(i)$ transmitted from the k_t^{th} transmit antenna on the component of $\underline{\boldsymbol{r}}_{m_1}(i)$ observed at the k_r^{th} receive antenna. Thus, off-diagonal entries of $\boldsymbol{\mathcal{H}}_{k_r,k_t}(i)$ cause ICI. (See [15], [17], [18] for an expression relating $\boldsymbol{\mathcal{H}}_{k_r,k_t}$ to the channel impulse response.)

A direct consequence of the employed coding strategy is that blocks of observations for N_b OFDM symbols are processed together and sub-carriers are decoded individually at the receiver. Using the entire observation $\boldsymbol{r}(i)$ to decode the k^{th} sub-carrier, however, requires prohibitively high complexity. Recalling that the Rayleigh Doppler spectrum is low-pass, however, it can be assumed that the ICI due to a sub-carrier is significant only within a radius of D_h adjacent sub-carriers, where $D_h = \lceil f_{\mathsf{d}} T_c N \rceil$. In this case, the significant entries of the MIMO-FDCM $\boldsymbol{H}(i)$ will be located in the quasi-block-banded region depicted in Fig. 1. To exploit this MIMO-FDCM structure, we employ the reception strategy of [19]. In this strategy, only $\boldsymbol{r}_k(i) := \left[\underline{\boldsymbol{r}}^T_{<k-D_h>_N}(i), \cdots, \underline{\boldsymbol{r}}^T_{<k+D_h>_N}(i)\right]^T$ is used to process the k^{th} sub-carrier. Further, the structure of the MIMO-FDCM dictates that $\boldsymbol{r}_k(i)$ sees significant ICI from sub-carriers with indices in the set $\mathcal{K}_k = \{< k \pm 1 >_N, \cdots, < k \pm 2D_h >_N\}$ only. The ICI from non-neighboring sub-carriers is relatively insignificant and can be neglected. Then $\boldsymbol{r}_k(i)$ can be written in terms of the information symbols as

$$\boldsymbol{r}_k(i) \;=\; \sum_{k' \in \mathcal{K}_k} \boldsymbol{H}_{k,k'}(i)\boldsymbol{x}_{k'}(i)s_{k'}(i) + \boldsymbol{w}_k(i), \quad (4)$$

where $\boldsymbol{H}_{k,k'}(i) \in \mathbb{C}^{(2D_h+1)N_r \times N_t}$ represents the influence of $\underline{\boldsymbol{t}}_{k'}(i) = \boldsymbol{x}_{k'}(i)s_{k'}(i)$ on $\boldsymbol{r}_k(i)$, and where $\boldsymbol{w}_k(i)$ is comprised of noise samples that affect $\boldsymbol{r}_k(i)$, so that $\boldsymbol{\Sigma}_{\boldsymbol{w}_k} = \sigma^2 \boldsymbol{I}_{(2D_h+1)N_r}$. In the reception strategy considered, local linear combining (LLC) is performed for the first sub-carrier ($k = 0$) for each of the N_b blocks. The obtained symbol estimates are fed to the decoder. Assuming judicious rate allocation and consequent error-free decoding, the interference due to the first sub-carrier can be regenerated and removed from observations for neighboring sub-carriers that it influences significantly. This process is called partial sequential interference cancellation (P-SIC). These steps are then repeated for the second ($k = 1$) sub-carrier, and so on. The effect of P-SIC on $\boldsymbol{r}_k(i)$ can be represented as

$$\boldsymbol{y}_k(i) \;=\; \boldsymbol{r}_k(i) - \sum_{k' \in \mathcal{K}_k^-} \boldsymbol{H}_{k,k'}(i)\boldsymbol{x}_{k'}(i)s_{k'}(i) \quad (5)$$

$$\;=\; \sum_{k' \in \mathcal{K}_k^+ \cup \{k\}} \boldsymbol{H}_{k,k'}(i)\boldsymbol{x}_{k'}(i)s_{k'}(i) + \boldsymbol{w}_k(i). \quad (6)$$

In (5) and (6), the set of sub-carrier indices $\mathcal{K}_k^-$ and $\mathcal{K}_k^+$ are defined as $\mathcal{K}_k^- = \mathcal{K}_k \cap \{l : l < k\}$ and $\mathcal{K}_k^+ = \mathcal{K}_k \cap \{l : l > k\}$, respectively. LLC for the k^{th} sub-carrier with local combiner (LC) $\boldsymbol{z}_k(i)$ can be written as

$$\phi_k(i) \;=\; \boldsymbol{z}_k^H(i)\boldsymbol{y}_k(i). \quad (7)$$

This paper presents novel approaches for the design of BVs $\{\boldsymbol{x}_k(i)\}_{k=0}^{N-1}$ and LCs $\{\boldsymbol{z}_k(i)\}_{k=0}^{N-1}$ using the simplified system model in (4) with the aim of (approximately) maximizing the (ergodic) achievable rate (AR) for the system. As a result of using (4), the BV and LC designs as well as all receiver processing use only a few neighboring significant ICI coefficients. (See Fig. 1.) As BVs and LCs are separately designed for each OFDM symbol, we consider an arbitrary OFDM symbol and drop the OFDM symbol indices for brevity. Using [19], the AR for this system can be shown to be

$$R \;=\; \mathrm{E}_{\boldsymbol{H}}\left(\sum_{k=0}^{N-1} \frac{\log\left(1+\gamma_k\right)}{N + N_h - 1}\right), \quad (8)$$

where the signal to interference-plus-noise ratio (SINR) for the k^{th} sub-carrier (after LLC) is given by

$$\gamma_k \;=\; \frac{\boldsymbol{z}_k^H \boldsymbol{H}_{k,k}\boldsymbol{x}_k\boldsymbol{x}_k^H\boldsymbol{H}_{k,k}^H\boldsymbol{z}_k}{\boldsymbol{z}_k^H\left(\sum_{k' \in \{\bar{\mathcal{K}}_k \cup \mathcal{K}_k^+\}} \boldsymbol{H}_{k,k'}\boldsymbol{x}_{k'}\boldsymbol{x}_{k'}^H\boldsymbol{H}_{k,k'}^H + \boldsymbol{\Sigma}_{\boldsymbol{w}_k}\right)\boldsymbol{z}_k} \quad (9)$$

In (9), the set $\bar{\mathcal{K}}_k = \{0, 1, \cdots, N-1\} \setminus \{\mathcal{K}_k \cup \{k\}\}$ is the set of non-neighboring sub-carriers whose ICI is neglected during the receiver processing for the k^{th} sub-carrier. In the next section, we present the LC and BV designs.

III. Combiner and Beamforming Vector Designs

An LC design for a given set of BVs is presented in Sec. III-A, a BV design is presented in Sec. III-B, and a joint LC/BV design is presented in Sec. III-C.

A. Local Combiner Design

Here, we design LCs $\{\boldsymbol{z}_k\}_{k=0}^{N-1}$ to (approximately) maximize the AR given a set of BVs $\{\boldsymbol{x}_k\}_{k=0}^{N-1}$. In this regard, notice that LC $\boldsymbol{z}_k$ does not affect $\{\gamma_l\}_{l\neq k}$. Then maximizing the AR *w.r.t.* LC $\boldsymbol{z}_k$ reduces to maximizing γ_k. However, realize that, in (9), the ICI from neighboring sub-carriers ($k' \in \mathcal{K}_k^+$) will dominate the ICI from non-neighboring sub-carriers ($k' \in \bar{\mathcal{K}}_k$). Also, recall that $\boldsymbol{\Sigma}_{\boldsymbol{w}_k} = \sigma^2\boldsymbol{I}$. Thus, the SINR γ_k can be approximated as

$$\gamma_k \;=\; \frac{\boldsymbol{z}_k^H\boldsymbol{H}_{k,k}\boldsymbol{x}_k\boldsymbol{x}_k^H\boldsymbol{H}_{k,k}^H\boldsymbol{z}_k}{\boldsymbol{z}_k^H\Big(\sum\limits_{k'\in\mathcal{K}_k^+}\boldsymbol{H}_{k,k'}\boldsymbol{x}_{k'}\boldsymbol{x}_{k'}^H\boldsymbol{H}_{k,k'}^H+\sigma^2\boldsymbol{I}\Big)\boldsymbol{z}_k}. \quad (10)$$

It is well known that γ_k in (10) is maximized by the choice

$$\boldsymbol{z}_k \;=\; \alpha_k\Big(\sum_{k'\in\mathcal{K}_k^+}\boldsymbol{H}_{k,k'}\boldsymbol{x}_{k'}\boldsymbol{x}_{k'}^H\boldsymbol{H}_{k,k'}^H+\sigma^2\boldsymbol{I}\Big)^{-1}\boldsymbol{H}_{k,k}\boldsymbol{x}_k, \quad (11)$$

where *w.l.o.g.*, we choose α_k to ensure $||\boldsymbol{z}_k|| = 1$. We use (11) to design all LCs in this paper.

B. Max-SNR Beamforming for DS Channels

Traditional BV designs for MIMO-OFDM over time invariant channels maximize sub-carrier SNRs. A similar max-SNR BV design is possible for MIMO-OFDM over DS channels, too. However, the DS channel spreads the energy of each sub-carrier into neighboring sub-carriers. Taking this spreading into account, the max-SNR BV can be written as the principal eigenvector of the matrix $\boldsymbol{H}_{k,k}^H\boldsymbol{H}_{k,k}$, *i.e.*

$$\boldsymbol{x}_k = \boldsymbol{\nu}_*(\boldsymbol{H}_{k,k}^H\boldsymbol{H}_{k,k}). \quad (12)$$

The solution in (12) is called the max-SNR-DS BV design. The designed BV $\boldsymbol{x}_k$ maximizes the energy from s_k in ϕ_k. However, in doing so, the max-SNR-DS BVs potentially increase the ICI caused to neighboring sub-carriers (i.e., energy from s_k in $\{\phi_l\}_{l\neq k}$). Therefore, performance can be improved if ICI suppression can be incorporated into the BV design process. In Sec. III-C, we propose one such solution.

C. Approximate Max-AR Beamforming and Combining

In this section, BVs and LCs are jointly designed to (approximately) maximize the AR. First, we consider the design of BVs given a set of LCs $\{\boldsymbol{z}_k\}_{k=0}^{N-1}$. Realize that each BV $\boldsymbol{x}_k$ affects several $\{\gamma_l\}_{l\neq k}$ and directly computing $\boldsymbol{x}_k$ to maximize the AR in (8) is difficult. Instead, we intuit properties of AR-optimal BVs and use these to construct an alternative cost function that is optimized to calculate the BVs. In this regard, notice that ϕ_k in (7) has a "signal" component ϕ_k^{s} and an "ICI plus noise" component ϕ_k^{i} given by

$$\phi_k^{\mathsf{s}} \;=\; \boldsymbol{z}_k^H\boldsymbol{H}_{k,k}\boldsymbol{x}_k\boldsymbol{s}_k, \quad (13)$$

$$\phi_k^{\mathsf{i}} \;=\; \boldsymbol{z}_k^H\Big(\sum_{k'\in\mathcal{K}_k^+}\boldsymbol{H}_{k,k'}\boldsymbol{x}_{k'}s_{k'}+\boldsymbol{w}_k\Big). \quad (14)$$

Then $\gamma_k = \mathrm{E}(|\phi_k^{\mathsf{s}}|^2)/\,\mathrm{E}(|\phi_k^{\mathsf{i}}|^2)$, where the expectations are taken over the joint source-noise distribution. Observe that BV $\boldsymbol{x}_k$ appears in ϕ_k^{s} and in $\{\phi_l^{\mathsf{i}}\}_{l\in\mathcal{K}_k^-}$. Now, realize that, in the low SNR regime, additive noise overshadows uncanceled ICI in (10). Hence, (10) can be approximated as

$$\gamma_k \;\approx\; \frac{\boldsymbol{x}_k^H\boldsymbol{H}_{k,k}^H\boldsymbol{z}_k\boldsymbol{z}_k^H\boldsymbol{H}_{k,k}\boldsymbol{x}_k}{\sigma^2||\boldsymbol{z}_k||^2}. \quad (15)$$

Then $\boldsymbol{x}_k$ only affects γ_k. Thus, an AR-optimal BV $\boldsymbol{x}_k$ should maximize $\mathrm{E}(|\phi_k^{\mathsf{s}}|^2)$. On the other hand, uncanceled ICI outweighs noise at high SNR. In this case, an AR-optimal BV $\boldsymbol{x}_k$ should maximize $\mathrm{E}(|\phi_k^{\mathsf{s}}|^2)$ and minimize each element of $\{\mathrm{E}(|\phi_l^{\mathsf{i}}|^2)\}_{l\in\mathcal{K}_k^-}$ simultaneously.

These intuitions suggest that a "good" BV should maximize $\mathcal{E}_s(k)$ and minimize $\mathcal{E}_{ni}(k)$ simultaneously, where

$$\mathcal{E}_s(k) \;=\; \mathrm{E}\left(|\boldsymbol{z}_k^H\boldsymbol{H}_{k,k}\boldsymbol{x}_k s_k|^2\right), \quad (16)$$

$$\mathcal{E}_{ni}(k) \;=\; \mathrm{E}\Big(\Big|\sum_{k'\in\mathcal{K}_k^-}\boldsymbol{z}_{k'}^H\boldsymbol{H}_{k',k}\boldsymbol{x}_k s_k+\boldsymbol{z}_k^H\boldsymbol{n}_k\Big|^2\Big). \quad (17)$$

This prompts us to define the cost function $\Gamma_b(k) = \mathcal{E}_s(k)/\mathcal{E}_{ni}(k)$. Recalling that $||\boldsymbol{z}_k|| = 1 = ||\boldsymbol{x}_k||$ from Sec. II and Sec. III-A, the cost function can be simplified to

$$\Gamma_b(k) = \frac{\boldsymbol{x}_k^H\boldsymbol{H}_{k,k}^H\boldsymbol{z}_k\boldsymbol{z}_k^H\boldsymbol{H}_{k,k}\boldsymbol{x}_k}{\boldsymbol{x}_k^H\Big(\sum\limits_{k'\in\mathcal{K}_k^-}\boldsymbol{H}_{k',k}^H\boldsymbol{z}_{k'}\boldsymbol{z}_{k'}^H\boldsymbol{H}_{k',k}+\sigma^2\boldsymbol{I}_{N_t}\Big)\boldsymbol{x}_k}. \quad (18)$$

Given a set of LCs $\{\boldsymbol{z}_k\}_{k=0}^{N-1}$, the $\Gamma_b(k)$-optimal BV is

$$\boldsymbol{x}_k = \beta_k\Big(\sum_{k'\in\mathcal{K}_k^-}\boldsymbol{H}_{k',k}^H\boldsymbol{z}_{k'}\boldsymbol{z}_{k'}^H\boldsymbol{H}_{k',k}+\sigma^2\boldsymbol{I}_{N_t}\Big)^{-1}\boldsymbol{H}_{k,k}^H\boldsymbol{z}_k, \quad (19)$$

where β_k can be chosen *w.l.o.g.* to ensure $||\boldsymbol{x}_k|| = 1$.

Combining the LC design from Sec. III-A and the BV design above, we propose an iterative approximate max-AR (AMAR) algorithm as follows. The algorithm is initialized by choosing a set of BVs $\{\boldsymbol{x}_k^{(0)}\}_{k=0}^{N-1}$ For our experiments, we found that the max-SNR-DS initialization

$$\boldsymbol{x}_k^{(0)} \;=\; \boldsymbol{\nu}_*(\boldsymbol{H}_{k,k}^H\boldsymbol{H}_{k,k}) \quad (20)$$

leads to good results. Each iteration $n_i \in \{1,\ldots,N_i\}$ consists of two stages. First, LCs $\{\boldsymbol{z}_k^{(n_i)}\}_{k=0}^{N-1}$ are computed using BVs $\{\boldsymbol{x}_k^{(n_i-1)}\}_{k=0}^{N-1}$ via (11). Next, BVs $\{\boldsymbol{x}_k^{(n_i)}\}_{k=0}^{N-1}$ are recalculated using the new LCs $\{\boldsymbol{z}_k^{(n_i)}\}_{k=0}^{N-1}$ via (19). The system then uses $\{\boldsymbol{z}_k^{(N_i)}\}_{k=0}^{N-1}$ and $\{\boldsymbol{x}_k^{(N_i)}\}_{k=0}^{N-1}$ as the BVs and LCs, respectively.

It is easy to see that the LC design complexity is $\mathcal{O}\left((2D_h+1)^3N_r^3NN_i\right)$ per MCM symbol, whereas the BV

design complexity is $\mathcal{O}\left(N_t^3 N\right)$ per MCM symbol, for a (N_t, N_r, N) MIMO-OFDM system. Thus, the complexity of the AMAR algorithm has the same scaling *w.r.t.* the number of sub-carriers N, the number of transmit antennas N_t and the number of receive antennas N_r as traditional max-SNR designs for MIMO-OFDM over time-invariant channels [11]–[13].

IV. Numerical Results and Discussion

In this section, we present numerical experiments that verify the utility of our designs. Specifically, we measure, using (8), the AR of a MIMO-OFDM system that employs our designs. Tests are performed on a $(N_t, 2, 128)$ MIMO-OFDM system. Transmission is over channels with $N_h = 16$ chip delay spreads and uniform power profiles, and each data point is an average of measurements for 10^3 channel realizations. In all our experiments, we compare our schemes, *i.e.*, the max-SNR-DS BVs from Sec. III-B and LCs from Sec. III-A (labeled as MSNR-DS) and the joint AMAR BVs and LCs from Sec. III-C (labeled as AMAR), to two benchmarks. First, we compare our designs with ICI-ignoring max-SNR beamforming and combining (labeled as MSNR), intended for time-invariant channels, from [11]–[13]. Second, we also compare our designs with an upper bound (labeled as UB). The upper bound corresponds to performance on a system using max-SNR-DS BVs, where the receiver, aided by a genie, *cancels all ICI perfectly*. Thus, such a receiver harnesses all available Doppler diversity while completely avoiding the ill effects of ICI.

Fig. 2 shows a plot of achievable rate versus sub-carrier SNR for (a) $N_t = 4$, (b) $N_t = 6$ and (c) $N_t = 8$ transmit antennas, respectively, and a (chip normalized single-sided) maximum Doppler spread of $f_{\mathsf{d}} T_c = 0.008$, so that $D_h = 1$. The results show that both of our designs are significantly superior to ICI-ignoring max-SNR designs. The iterative AMAR design provides additional rate gains over the max-SNR-DS design at the expense of slightly higher design complexity. Further, our designs perform close to the UB at low and moderate SNRs. On the other hand, neglecting strong ICI components creates a significantly lower performance ceiling for the ICI ignoring max-SNR schemes. When the SNR is high, the gap between the UB and the performance of both our proposed schemes grows due to uncanceled out-of-band ICI. However, out-of-band ICI produces pronounced performance degradation at very high SNRs that may be beyond the normal operating SNR range of most practical systems. Finally, we observe that performance can be enhanced by increasing the number of transmit antennas. This is expected as more transmit antennas provide more freedom to the BV designs in choosing directions rich in signal energy and low in interference energy.

Next, we study the effect of Doppler spread (i.e., mobility) on our system. First, realize that when there is no Doppler spread ($D_h = 0$), our designs reduce to a max-SNR design and hence, perform optimally. A plot of achievable rate versus sub-carrier SNR can be found in Fig. 3 for $N_t = 4$ transmit antennas and a maximum Doppler spread of (a) $f_{\mathsf{d}} T_c = 0.008$ ($D_h = 1$), and (b) $f_{\mathsf{d}} T_c = 0.016$ ($D_h = 2$), respectively. These could correspond to, for instance, a channel with bandwidth of 1.5MHz, carrier frequency of 60GHz, delay spread of 10.8 μs, and mobile and reflector velocities of (a) 69 km/hr and (b) 138 km/hr, respectively, in a "triple Doppler" scenario [20].

The assumption of transmit CSI may be unrealistic for a rapidly varying channel. However, approximate transmit CSI can be attained in systems operating in a time division duplex (TDD) mode via prediction from channel measurements made during the previous TDD epoch. To test this idea, we assume that, when in reception mode, the node has near-perfect CSI (via, e.g., pilot aided or decision directed estimation). The node then predicts the channel for the next OFDM symbol duration, when it operates as a transmitter. A MMSE channel predictor that exploits the correlation structure arising from the the WSSUS Rayleigh fading is used. In Fig. 3, traces labeled MSNR-DS-P and AMAR-P refer to versions of the max-SNR-DS BV design and the joint AMAR design, respectively, that use predicted transmitter CSI. The general trends are similar to that of Fig. 2. In addition, we observe that, whereas our schemes adapt well to channels with large Doppler spreads, the max-SNR design loses significantly. This behavior results from the fact that the max-SNR scheme completely neglects ICI. Furthermore, we see that, even in a highly mobile environment with large Doppler spreading, the predicted-CSI case achieves rates only slightly less than the perfect-CSI case. This establishes the robustness of our designs to imperfect transmitter CSI.

V. Conclusion

In this paper, we presented BV and LC designs for MIMO-OFDM appropriate for high mobility scenarios. Three novel designs: a SNR maximizing BV design, an AR maximizing LC design, and a joint AMAR design, were discussed. Numerical experiments suggest that our designs provide large gain over traditional designs, and remain robust to large Doppler spreads and predicted transmitter CSI, in spite of having the same complexity orders as traditional designs. Thus, they provide attractive alternatives to traditional ICI-ignoring beamformers/combiners for MIMO-OFDM systems.

References

[1] V. Tarokh, N. Seshadri, and A. R. Calderbank, "Space-time codes for high data rate wireless communications: Performance criterion and code construction," *IEEE Trans. Inform. Theory*, vol. 44, pp. 744–765, Mar. 1998.

[2] V. Tarokh, H. Jafarkhani, and A. R. Calderbank, "Space-time block codes from orthogonal designs," *IEEE Trans. Inform. Theory*, vol. 45, pp. 1456–1467, July 1999.

[3] T. K. Y. Lo, "Maximum ration transmission," *IEEE Trans. Commun.*, vol. 47, pp. 1458–1461, Oct 1999.

[4] H. El Gamal, G. Caire, and M. O. Damen, "Lattice coding and decoding achieve the optimal diversity-multiplexing tradeoff of MIMO channels," *IEEE Trans. Inform. Theory*, vol. 30, pp. 968–985, June 2004.

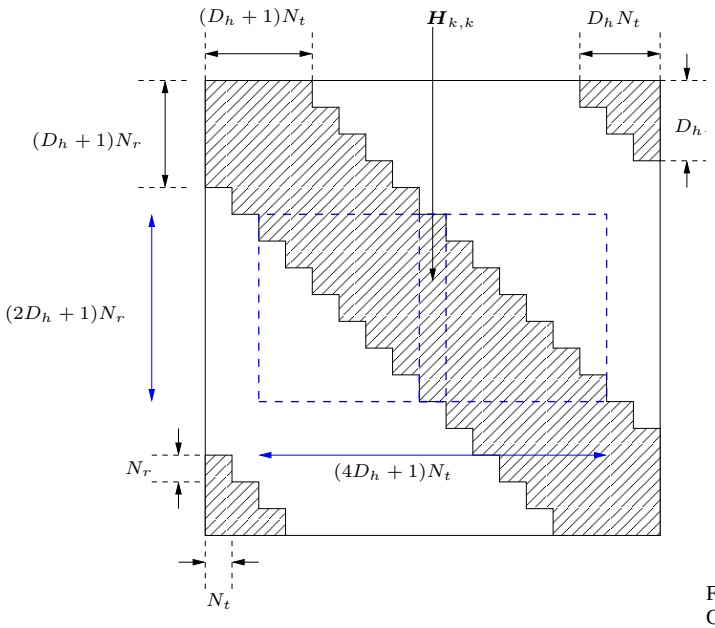

Fig. 1. Approximate structure of MIMO-FDCM. Rectangle (in dotted lines) indicates the channel coefficients used for processing/design of BVs for the k^{th} sub-carrier.

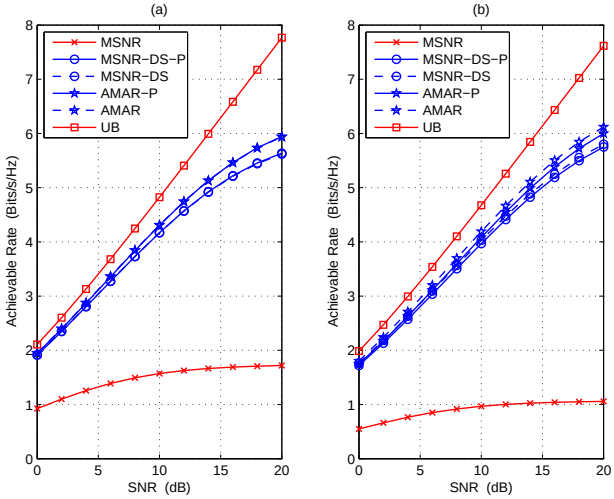

Fig. 3. Performance of BV designs on a system in TDD mode with predicted CSI at the transmitter for (a) $f_{\mathrm{d}}T_c = 0.008$, and (b)$f_{\mathrm{d}}T_c = 0.016$.

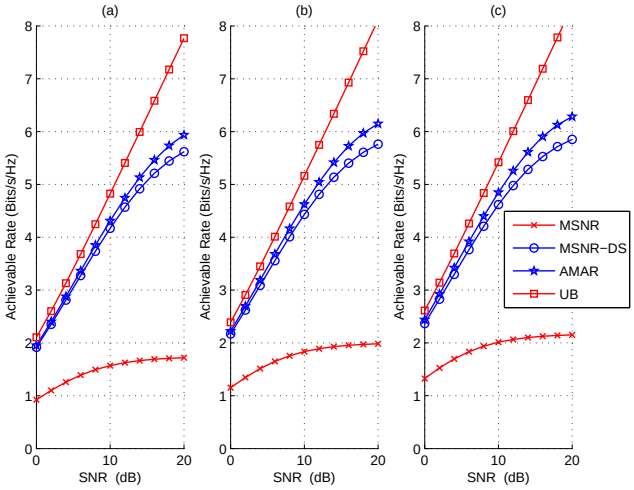

Fig. 2. Plot of Achievable Rate versus SNR for (a) $N_t = 4$, (b)$N_t = 6$ and (c)$N_t = 8$ transmit antennas.

[5] D. J. Love and R. W. Heath, Jr., "Equal gain transmission in multiple-input multiple-output wireless systems," *IEEE Trans. Commun.*, vol. 51, pp. 1102–1110, Jul 2003.

[6] B. Le Floch, M. Alard, and C. Berrou, "Coded orthogonal frequency division multiplex," *Proc. IEEE*, vol. 83, pp. 982–996, June 1995.

[7] R. Haas and J.-C. Belfiore, "A time-frequency well-localized pulse for multiple carrier transmission," *Wireless Personal Commun.*, vol. 5, pp. 1–18, 1997.

[8] W. Kozek and A. F. Molisch, "Nonorthogonal pulseshapes for multicarrier communications in doubly dispersive channels," *IEEE J. Select. Areas In Commun.*, vol. 16, pp. 1579–1589, Oct. 1998.

[9] H. Bölcskei, P. Duhamel, and R. Hleiss, "Design of pulse-shaping OFDM/OQAM systems for high data-rate transmission over wireless channels," in *Proc. IEEE Int. Conf. Commun.*, vol. 1, pp. 559–564, June 1999.

[10] J. A. C. Bingham, "Multicarrier modulation for data transmission: An idea whose time has come," *IEEE Commun. Mag.*, vol. 28, pp. 5–14, May 1990.

[11] H. Bölcskei, D. Gesbert, and A. J. Paulraj, "On the capacity of OFDM based spatial multiplexing systems," *IEEE Trans. Commun.*, vol. 50, pp. 225–234, Feb. 2002.

[12] H. Bölcskei, M. Borgmann, and A. J. Paulraj, "Impact of the propagation environment on the performance of space-frequency coded MIMO-OFDM," *IEEE J. Select. Areas In Commun.*, vol. 21, pp. 427–439, Apr. 2002.

[13] G. C. Raleigh and J. M. Cioffi, "Spatio-temporal coding for wireless communication," *IEEE J. Select. Areas In Commun.*, vol. 46, pp. 357–366, March 1998.

[14] A. Stamoulis, S. N. Diggavi, and N. Al-Dhahir, "Intercarrier interference in MIMO OFDM," *IEEE Trans. Signal Processing*, vol. 50, pp. 2451–2464, Oct. 2002.

[15] P. Schniter, "Low-complexity equalization of OFDM in doubly-selective channels," *IEEE Trans. Signal Processing*, vol. 52, pp. 1002–1011, Apr. 2004.

[16] X. Ma and G. B. Giannakis, "Maximum-diversity transmissions over doubly-selective wireless channels," *IEEE Trans. Inform. Theory*, vol. 49, pp. 1832–1840, July 2003.

[17] P. Schniter, "A new approach to multicarrier pulse design for doubly-dispersive channels," in *Proc. Allerton Conf. Commun., Control, and Computing*, Oct. 2003.

[18] S. Das and P. Schniter, "Max-SINR ISI/ICI-shaped multi-carrier communication over the doubly dispersive channel," *IEEE Trans. Signal Processing*, 2006. Submitted.

[19] S. Das and P. Schniter, "Design of multi-carrier modulation for doubly selective channels based on a complexity constrained achievable rate metric," in *Proc. Asilomar Conf. Signals, Systems and Computers*, Nov. 2006.

[20] T. A. Thomas, T. P. Krauss, and F. W. Vook, "CHAMPS: A near-ML joint doppler frequency / TOA search for channel characterization," in *Proc. IEEE Veh. Tech. Conf.*, Fall 2003.